scientific reports

Check for updates

OPEN

Characterization of microvessels in the human forehead dermis using intravascular dual perfusion and immunofluorescence staining

Shu Rui, Zilong Cao, Yunzhang Wang & Liqiang Liu✉

Skin microcirculation provides essential insights in clinical practice. However, the specific characteristics and distribution patterns of dermal microarterioles and microvenules remain insufficiently explored. This study aimed to analyze their structural differences and distribution in the human forehead skin using an innovative intravascular dual perfusion technique combined with immunofluorescence staining to distinguish microvessel types within the dermis. Using two post-mortem cadaver specimens, lead oxide-gelatin perfusion was applied to label microarterioles, and latex was used for microvenules. Tissue sections underwent hematoxylin and eosin and immunofluorescence staining, with cluster of differentiation 31 (CD31) serving as a general vascular marker and monocarboxylate transporter 1 (MCT1) as a venule-specific marker. The analysis revealed significant structural differences between dermal layers: vessels in the deep dermis had larger diameters and thicker walls than those in the superficial layer, while microvessel density was higher in the superficial dermis. These findings demonstrate distinct patterns and significant differences in microvessel distribution between the superficial and deep dermal layers, reflecting their layer-specific functional demands. Furthermore, MCT1 was identified as a specific marker for microvenules, and a novel method combining CD31 and MCT1 immunofluorescent staining was introduced to differentiate dermal microarterioles from microvenules. These results offer valuable implications for surgical planning, skin grafting, and diagnostics related to microcirculation.

Keywords Skin microcirculation, Dermal microvessels, Intravascular perfusion, MCT1, Immunofluorescence staining, Frontal flap

Skin microcirculation plays a crucial role in clinical practice, providing important insights into biological processes in both health and disease. It helps clinicians understand the vascular mechanisms underlying various systemic diseases, such as metabolic disorders[1–3], cardiovascular conditions[4–6], immune system diseases[7–10], renal diseases[11,12], and skin aging[13,14]. Furthermore, research on skin microcirculation is vital for skin surgeries and tissue engineering[15]. In particular, the success of flap surgeries, including blood flow and recovery, is closely linked to the density and distribution of microvessels[16–18]. Two main strategies for improving flap survival—venous superdrainage and arterial superperfusion—focus on enhancing venous outflow[19] and arterial blood supply[20,21], respectively. However, a lack of comprehensive understanding of skin microvessels has led to ongoing debates about the effectiveness of these strategies.

Each layer of the skin serves a distinct function, with the dermis playing a key role in supporting the network of microvessels that supply nutrients and oxygen[22]. A clear understanding of the microvessel distribution within the dermis is essential to comprehend skin microcirculation. Morphologically, the dermis is divided into the upper papillary dermis and the deeper reticular dermis. The papillary dermis, located just beneath the epidermis, consists of loose connective tissue, while the reticular dermis, which makes up most of the dermis, is composed of denser connective tissue that provides structural support to the skin[23,24]. These structural differences define the unique functions of each dermal layer. However, the precise distribution and characteristics of microvessels across different dermal layers remain inadequately explored. Current research on skin microcirculation often treats microvessels as a single entity, with little differentiation between microarterioles and microvenules. Some studies have proposed methods to distinguish small arterioles and venules in human tissue pathology, but these

Plastic Surgery Hospital, Chinese Academy of Medical Sciences and Peking Union Medical College, Beijing, China. ✉email: liuliqiang@psh.pumc.edu.cn

methods have had limited success when applied to dermal microvessels[25–28]. In 2019, Deegan and Wang[29] reviewed microvascular imaging of skin using optical coherence tomography angiography (OCTA), finding changes in vessel density at different dermal depths, including the papillary dermis, upper reticular dermis, and reticular dermis, but without distinguishing between arterioles and venules. Similarly, other techniques, such as indocyanine green angiography[30], computed tomography angiography[17,31], and tissue optical clearing[32], have proven insufficient for distinguishing dermal microarterioles from microvenules. In 2018, Vanlandewijck et al.[33] used single-cell transcriptomics in adult mice to identify molecular markers for arterioles and venules, identifying monocarboxylate transporter 1 (MCT1) as a potential marker for venules and capillaries. Cao et al.[34] later confirmed that MCT1 immunohistochemical staining can effectively differentiate small venules from arterioles in human brain tissue. However, MCT1's applicability in distinguishing microvessels in the human dermis has not yet been verified.

Given the limitations of current techniques in differentiating dermal microarterioles from microvenules and understanding their spatial distribution, we designed this study to address these gaps. We used intravascular perfusion of post-mortem forehead skin specimens. The frontal flap, commonly used for facial and neck reconstruction, often faces complications like distal congestion and necrosis[35]. Mapping the microvessel distribution could clarify the effectiveness of superperfusion and superdrainage strategies and offer insights for other skin studies. Vascular perfusion is a traditional technique for visualizing blood vessels using materials such as lead oxide, barium carbonate, latex, and ink[36–40]. The micron-sized particles of lead oxide and latex can theoretically reach the microvascular level of dermal arterioles and venules[39,41–43]. Previous studies using lead oxide perfusion have successfully visualized arteriovenous anastomoses[44] and the connection between the facial artery and adjacent vessels[45]. In our study, we used selective perfusion solutions to label microarterioles and microvenules, followed by hematoxylin and eosin (H&E) staining and immunofluorescence to analyze their distribution within the dermal layers. By comparing the expression of MCT1 and cluster of differentiation 31 (CD31), we evaluated MCT1 as a specific marker for microvenules and developed a reliable method to distinguish between different types of microvessels in the dermis.

Material and methods

Cadaver donors

The study utilized two freshly donated cadaver specimens from the Department of Human Anatomy, Histology and Embryology, Peking Union Medical College, with approval from the Chinese Academy of Medical Sciences and Peking Union Medical College. The experiments were reviewed and approved by the Ethics Committee of the Plastic Surgery Hospital, Chinese Academy of Medical Sciences, in compliance with the Declaration of Helsinki principles. Both donors voluntarily donated their bodies, and the specimens were obtained within 24 h post-mortem. Perfusion attempts on specimens obtained beyond this timeframe or on formalin-fixed tissues were unsuccessful due to endothelial cell necrosis, increased fragility of microvasculature, compromised structural integrity, or peripheral vascular thrombosis. Detailed information about the specimens is provided in Table 1. The facial and scalp soft tissues were intact in all specimens, with no history of craniofacial trauma or surgery.

Surgical procedure and intravascular dual perfusion protocol

A longitudinal incision was made in the preauricular area on both sides to expose the superficial temporal fascia. The superficial temporal artery and vein were carefully dissected. A 20G needle was inserted into the artery and a 19G needle into the vein, respectively, both secured with 4–0 nylon sutures. Next, an incision was made along the supraorbital ridge, extending to the occipital protuberance and down to the cranial surface. A bone saw was used to cut through the scalp-cranium composite tissue, while preserving the preauricular soft tissue to ensure the integrity of the superficial temporal artery and vein. For the perfusion, an arterial solution was prepared using lead oxide-gelatin: 100 g of red lead oxide (Sigma-Aldrich, St. Louis, MO, USA, Cat# 241547), 100 ml of 0.9% NaCl solution (Thermo Fisher Scientific, Waltham, MA, USA, Cat# BR0053G) , and 5 g of gelatin (Sigma-Aldrich, St. Louis, MO, USA, Cat# 1288485) . The mixture was heated to 60 °C and stirred until dissolved. For venous perfusion, latex (Sigma-Aldrich, St. Louis, MO, USA, Cat# LB11) was diluted 1:5 with 0.9% NaCl solution to reduce viscosity, and heated to 60 °C. The superficial temporal veins were clamped bilaterally, and arterial perfusion was initiated by injecting the solution at 20 mL/min using a 20 mL syringe. Perfusion continued until the solution exited the contralateral artery. The contralateral artery was clamped, and an additional 10 mL of solution was injected slowly until the perfused skin area turned orange. The same procedure was repeated for venous perfusion. After perfusion, the scalp-cranium specimens were frozen at − 20 °C for 60 min to solidify the perfusion solution. Finally, the forehead skin specimens were carefully excised from the periosteum and fixed in 4% paraformaldehyde for 48 h.

Tissue staining

The tissue samples were dehydrated using graded ethanol solutions and cleared with xylene, followed by paraffin embedding and sectioning at 5 µm thickness. After deparaffinization in xylene and rehydration through a graded

Serial No	Age (Years)	Gender	Cause of death	Perfused vessels
1	40	Male	Liver cancer	Left superficial temporal artery, superficial temporal vein
2	78	Male	Myocardial infarction	Right superficial temporal artery, superficial temporal vein

Table 1. Basic data of cadaver specimens.

ethanol series (100%, 95%, 85%, and 70%), the sections were transferred to distilled water. Hematoxylin staining was performed for 5 min, followed by rinsing under running water. The sections were briefly differentiated in 0.5% acid alcohol, blued with 0.25% ammonia water, rinsed, and counterstained with eosin for 2 min. After final dehydration and clearing, the sections were mounted with neutral balsam. Microvascular structures were assessed under a light microscope, and slide scanning was performed using the NanoZoomer 2.0-RS slide scanner (Hamamatsu Photonics, Hamamatsu, Japan).

Immunofluorescence staining was performed on adjacent sections of H&E-stained slides to evaluate the expression of MCT1 and CD31. Sections were baked at 60 °C for 1 h to remove paraffin, followed by standard dewaxing and rehydration through xylene and graded ethanol solutions. Antigen retrieval was conducted using heat-induced epitope retrieval in citrate buffer (pH 6.0) under high pressure for 10 min. After cooling and PBS rinses, sections were blocked with 5% BSA in PBS for 1 h to minimize nonspecific binding. Primary antibodies—rabbit anti-MCT1 (Abcam, Cambridge, UK, Cat# ab315382, 1:200) and mouse anti-CD31 (Abcam, Cambridge, UK, Cat# ab9498, 1:100)—were applied, and sections were incubated overnight at 4 °C. The following day, sections were washed with PBS and incubated with secondary antibodies—Cy3-conjugated goat anti-rabbit IgG (Jackson ImmunoResearch, West Grove, PA, USA, 1:500) and Alexa Fluor 488-conjugated goat anti-mouse IgG (Invitrogen, Carlsbad, CA, USA, 1:500)—for 1 h in the dark. DAPI was subsequently used to stain nuclei, aiding in the spatial visualization of the fluorescence signals. Finally, slides were mounted with anti-fade mounting medium. The stained sections were observed and imaged using an Olympus IX 81 confocal microscope (FluoView 300, Olympus, Tokyo, Japan). Fluorescence intensity was quantitatively analyzed using ImageJ software version 1.48 (NIH, Bethesda, MD, USA).

Microscopic analysis and quantification

The stained tissue sections were independently reviewed by two pathologists, and 40 fields of view were selected for analysis. In H&E-stained sections, we assessed the number of microarterioles and microvenules in both superficial and deep dermal layers, as well as vessel diameter and wall thickness. The superficial dermis (papillary layer) contains loose connective tissue with small blood vessels for nutrient exchange with the epidermis, while the deep dermis (reticular layer) comprises denser connective tissue and larger vessels that provide structural support and contain skin appendages, such as hair follicles and sweat glands[46]. To measure vessel diameter, we categorized vessels as cross-sectional or longitudinal based on their morphology in H&E-stained sections. Cross-sectional vessels appeared round or oval with uniform walls and clear boundaries, while longitudinal vessels showed elongated tubular shapes. For cross-sectional vessels, diameter was calculated as the square root of the product of the major and minor axes[47]. For longitudinal vessels, diameter was estimated as the lumen width perpendicular to the vessel's long axis. Microvessel density was determined by counting vessels per unit area (mm^2). Additionally, we analyzed the microarteriole-to-microvenule ratio, as well as the densities of each vessel type in the two dermal layers, to reveal distinct distribution patterns.

Statistical analysis

Data were analyzed using SPSS software version 26 (IBM SPSS Inc., Chicago, IL, USA). Continuous variables are presented as mean ± standard deviation (SD). The normality of the data was assessed using the Shapiro–Wilk test, which indicated that none of the variables significantly deviated from a normal distribution ($p > 0.05$). Therefore, independent samples t-tests were applied to compare continuous variables between groups. Statistical significance was set at $p < 0.05$.

Result

Intravascular dual perfusion process and skin specimen preparation

Intravascular perfusion of the superficial temporal vessels was effectively achieved in fresh cadavers, resulting in the skin within the perfused area turning orange, indicative of successful perfusion (Fig. 1a, b). The scalp-cranium specimens were subsequently obtained, and the scalp was carefully separated from the underlying structures for further analysis (Fig. 1c, d).

Distribution patterns and differences of microarterioles and microvenules in the dermis

In the H&E-stained sections of the perfused specimens, microarterioles appeared with black lumens due to lead oxide-gelatin perfusion, while microvenules displayed blue or light purple lumens resulting from latex perfusion (Fig. 2). Table 2 illustrates the distribution differences of microvessels between the superficial and deep dermis, focusing on parameters such as diameter, wall thickness, and density. Table 3 offers a detailed comparison of microarteriole and microvenule characteristics, including their structural differences and density variations across dermal layers.

The results revealed significant differences in microvascular diameters across dermal layers. The diameter of microarterioles in the superficial dermis measured 23.78 ± 3.88 μm, compared to 61.48 ± 23.69 μm in the deep dermis, demonstrating a statistically significant variation ($p < 0.001$, Table 2). Similarly, microvenule diameter was 40.85 ± 10.61 μm in the superficial dermis and 87.58 ± 19.27 μm in the deep dermis, also showing a significant difference ($p < 0.001$, Table 2). Across the entire dermis, distinct differences were observed in the diameters of microarterioles and microvenules, with microarterioles measuring 42.63 ± 25.37 μm and microvenules 64.21 ± 28.07 μm, both demonstrating statistically significant differences ($p < 0.001$, Table 3).

The findings also indicated significant differences in microvascular wall thickness between dermal layers. The wall thickness of microarterioles in the superficial dermis measured 3.83 ± 0.49 μm, compared to 25.03 ± 6.66 μm in the deep dermis, demonstrating a statistically significant difference ($p < 0.001$, Table 2). Similarly, microvenule wall thickness was 2.69 ± 0.45 μm in the superficial dermis and 5.04 ± 0.67 μm in the deep dermis, also showing a significant variation ($p < 0.001$, Table 2). When comparing the overall wall thickness of microarterioles and

Fig. 1. Intravascular dual perfusion and scalp-cranium specimen preparation. (**a**) Intravascular perfusion of the superficial temporal vessels, with orange discoloration indicating successful perfusion. (**b**) Scalp-cranium specimen obtained after perfusion. (**c**) Separation of the scalp from the underlying cranium. (**d**) Forehead skin tissue prepared for further analysis after perfusion.

microvenules across the entire dermis, the wall thickness of microarterioles was 14.43 ± 11.60 μm, while that of microvenules was 3.86 ± 1.31 μm, both demonstrating statistically differences ($p < 0.001$, Table 3).

The results further demonstrated significant differences in microvascular density across dermal layers. Microarteriole density in the superficial dermis was 1.96 ± 0.57 vessels/mm^2, compared to 1.71 ± 0.42 vessels/mm^2 in the deep dermis, indicating a statistically significant difference ($p = 0.026$, Table 2). Similarly, microvenule density was 2.88 ± 0.44 vessels/mm^2 in the superficial dermis and 2.29 ± 0.35 vessels/mm^2 in the deep dermis, also showing a significant layer-dependent difference ($p < 0.01$, Table 2). When comparing microarterioles and microvenules within each layer, a significant density difference was observed in the superficial dermis ($p < 0.001$, Table 3) and similarly in the deep dermis ($p < 0.001$, Table 3).

The ratio of microarterioles to microvenules showed no significant difference between the dermal layers. The microarteriole-to-microvenule ratio in the superficial dermis was 0.69 ± 0.22, while in the deep dermis it was 0.75 ± 0.18, with no statistically significant difference between the two layers ($p = 0.132$, Table 2).

MCT1 selectively marks microvenules, while CD31 labels both microarterioles and microvenules

The comparison of adjacent H&E and immunofluorescence-stained sections demonstrated that CD31 was positively expressed in the lumens of both microarterioles and microvenules. In contrast, MCT1 exhibited positive staining exclusively in a subset of microvenules perfused with latex, while no staining was observed in microarterioles perfused with lead oxide (Fig. 3). To further quantify, fluorescence intensity was measured as the relative fluorescence intensity ratio of MCT1–CD31 (MCT1/CD31). The analysis revealed that the relative fluorescence intensity in microarterioles was nearly zero, significantly lower than that in microvenules ($p < 0.001$, Fig. 4). These findings confirm that MCT1 is a specific marker for microvenules in dermal microvessels. Additionally, MCT1 showed positive expression in the lumens of certain sweat glands (Fig. 5).

Discussion

Current understanding of skin microcirculation anatomy is primarily built on the foundational work of Braverman and Keh-Yen[48–50]. Normal skin microcirculation consists of two vascular plexuses running parallel to

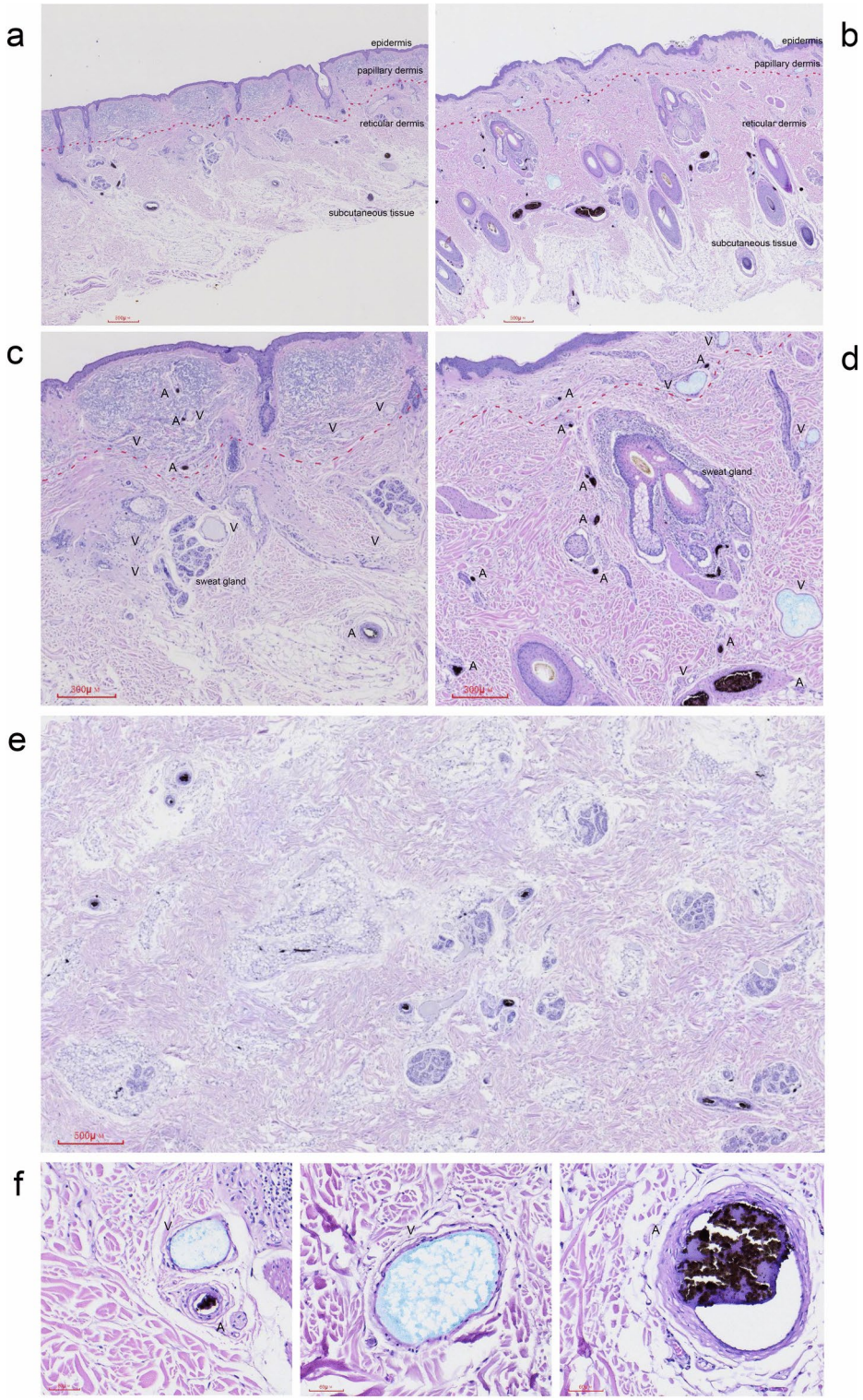

Fig. 2. Observation of microarterioles (A) and microvenules(V) in hematoxylin and eosin (H&E)-stained sections of perfused specimens. (**a**, **b**) Full-thickness vertical sections of the skin post-perfusion, showing microarterioles with black-filled lumens and microvenules with light purple or blue-filled lumens. (**c**, **d**) Magnified and close-up views of vertical sections, highlighting the distribution of microarterioles and microvenules in the papillary and reticular dermis. (**e**) Horizontal section parallel to the skin surface, showing perfused microvessels. (**f**) High-magnification images of microarterioles and microvenules, with black-filled lumens representing microarterioles and blue-filled lumens corresponding to microvenules. H&E: hematoxylin and eosin.

	Superficial dermis (40 fields of view)	Deep dermis (40 fields of view)	*p*-value
Microarteriole diameter (μm)	23.78 ± 3.88	61.48 ± 23.69	**< 0.001***
Microvenule diameter (μm)	40.85 ± 10.61	87.58 ± 19.27	**< 0.001***
Microarteriole wall thickness (μm)	3.83 ± 0.49	25.03 ± 6.66	**< 0.001***
Microvenule wall thickness (μm)	2.69 ± 0.45	5.04 ± 0.67	**< 0.001***
Microarteriole density (vessels/mm^2)	1.96 ± 0.57	1.71 ± 0.42	**0.026**
Microvenule density (vessels/mm^2)	2.88 ± 0.44	2.29 ± 0.35	**< 0.01***
Microarteriole-to-microvenule ratio	0.69 ± 0.22	0.75 ± 0.18	0.132

Table 2. Comparison of microvascular parameters between superficial and deep dermis layers. Significant values are in bold. *$p < 0.05$.

	Microarteriole (40 fields of view)	Microvenule (40 fields of view)	*p*-value
Diameter (μm)	42.63 ± 25.37	64.21 ± 28.07	< 0.001*
Wall thickness (μm)	14.43 ± 11.60	3.86 ± 1.31	< 0.001*
Superficial dermis density (vessels/mm^2)	1.96 ± 0.57	2.88 ± 0.44	< 0.001*
Deep dermis density (vessels/mm^2)	1.71 ± 0.42	2.29 ± 0.35	< 0.001*

Table 3. Comparison of parameters in microarteriole and microvenule. *$p < 0.05$.

the skin surface. The superficial plexus, located in the dermis, nourishes the skin, while the deep plexus, located at the dermal-subcutaneous interface, contains arteries and veins from the underlying muscle and fat tissue. These vessels penetrate the fascia forming ascending arterioles and descending venules, which connect with the superficial plexus[48–50]. Skin microcirculation often serves as an early indicator of systemic diseases[51]. For instance, Debbabi et al.[52] demonstrated that measuring skin microcirculation blood flow is a reliable, non-invasive method for assessing systemic endothelial function. In patients with chronic heart failure and hypertension, microvascular remodeling and dysfunction in the skin are frequently observed[53–55]. Similarly, in autoimmune diseases like systemic sclerosis, skin microvessels show capillary loss, dilation, and endothelial cell damage[56,57]. In psoriasis, dilated microvessels show neovascularization, offering insights into disease severity and treatment response[8,58]. Additionally, Schaper et al.[59] and Lee et al.[60] found that monitoring skin microvascular function in diabetic patients predicts severe complications such as diabetic foot ulcers and retinopathy. Additionally, Martens et al.[61] demonstrated an independent correlation between reduced skin microvessel density and glomerular proteinuria, while Orbegozo et al.[62] used laser Doppler to show that impaired microvascular reactivity in the forearm is a marker of circulatory shock severity. Furthermore, recent studies have explored the role of other dermal components, such as fibroblasts in the papillary and reticular dermis, in supporting vascular formation and regulation. Sorrell et al.[63] found that superficial dermal fibroblasts interact with endothelial cells to support microvascular formation, while papillary fibroblasts promote branching blood vessel structures. Philippeos et al.[64] further identified that papillary fibroblasts are linked to Wnt signaling, which is crucial for epidermal regeneration and wound healing. In contrast, reticular fibroblasts respond to interferon-γ (IFN-γ), supporting matrix reconstruction and fibrosis. Mauroux et al.[65] demonstrated that papillary fibroblasts promote angiogenesis, while reticular fibroblasts inhibit it, suggesting that fibroblasts in different dermal layers play distinct roles in blood vessel formation. These findings provide new insights for therapeutic approaches targeting microvessels in the dermis. However, distinguishing whether the observed changes occur in microarterioles or microvenules remains a challenge.

In plastic and dermatologic surgery, microcirculation plays a crucial role in determining surgical outcomes. Skin transplantation is commonly used to repair tissue defects caused by trauma, burns, or tumor resection. The analysis of dermal microvessels, both qualitatively and quantitatively, is essential for skin grafts, flap surgeries, prefabricated skin-flaps, and skin tissue engineering[15,66,67]. Preoperative identification of the distribution of microarterioles and microvenules helps optimize surgical planning. Postoperative monitoring, on the other hand, aids in managing complications such as venous congestion and insufficient flap perfusion, which promotes graft healing and recovery[68–70]. A clear understanding of the structure, distribution, and characteristics of microarterioles and microvenules is critical, as it aids surgeons in selecting appropriate donor arteries and veins to establish circulation in grafts. The frontal flap, often used for facial and neck reconstruction, is ideal due to its similar texture to the surrounding skin. However, distal congestion and necrosis are common postoperative complications[35]. These complications are closely related to microcirculatory dynamics, and the effects of superperfusion and superdrainage remain controversial due to insufficient morphological evidence regarding dermal arterioles and venules[71,72]. Understanding the distribution and structural differences of microarterioles and microvenules in the dermis may resolve these issues, improve surgical strategies, and guide postoperative care. Although various methods exist for studying skin microvessels, most focus on overall blood flow and do not differentiate between microarterioles and microvenules. Additionally, these methods do not analyze the spatial distribution of these vessels in detail[73,74]. Thus, our study aims to provide a deeper understanding of the dermal vascular network and its microcirculatory structure.

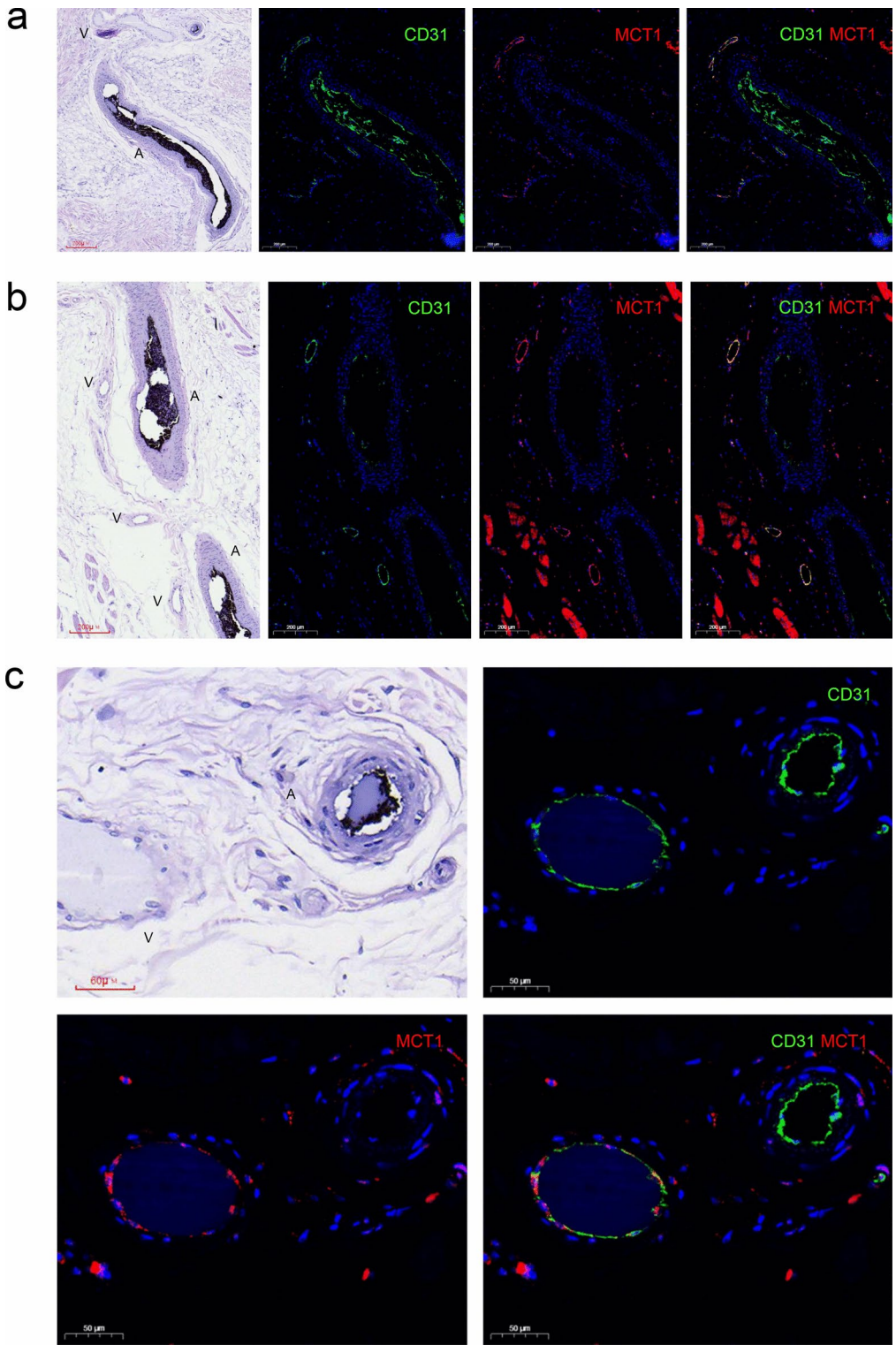

Fig. 3. Immunofluorescence and hematoxylin and eosin (H&E) staining of perfused microarterioles (A) and microvenules (V). (**a**) A microarteriole and a microvenule are shown, both showing CD31 positivity, while only the microvenule shows MCT1 positivity. (**b**) Three microvenules and two microarterioles observed, with MCT1 positivity restricted to the microvenules. Additionally, some sweat glands show MCT1 positivity. (**c**) A single microarteriole and microvenule, both positive for CD31, with MCT1 positivity confined to the microvenule. H&E: hematoxylin and eosin; CD31: cluster of differentiation 31; MCT1: monocarboxylate transporter 1.

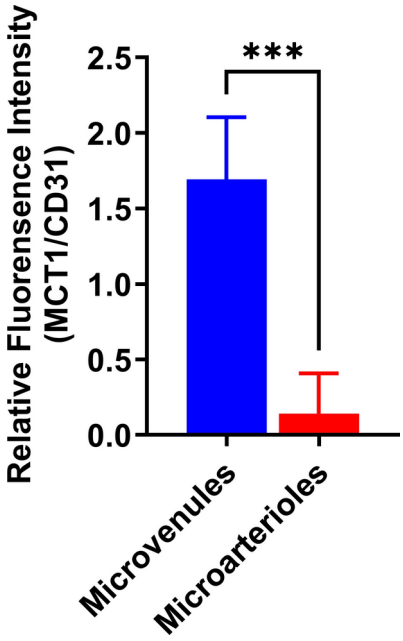

Fig. 4. Relative fluorescence intensity ratio of monocarboxylate transporter 1 (MCT1) to cluster of differentiation 31 (CD31) in microarterioles and microvenules. Immunofluorescence staining demonstrated that the MCT1/CD31 intensity in microarterioles was nearly zero, significantly lower than that in microvenules, confirming minimal MCT1 expression in microarterioles. *** indicates a statistically significant difference between groups ($p < 0.001$). CD31: cluster of differentiation 31; MCT1: monocarboxylate transporter 1.

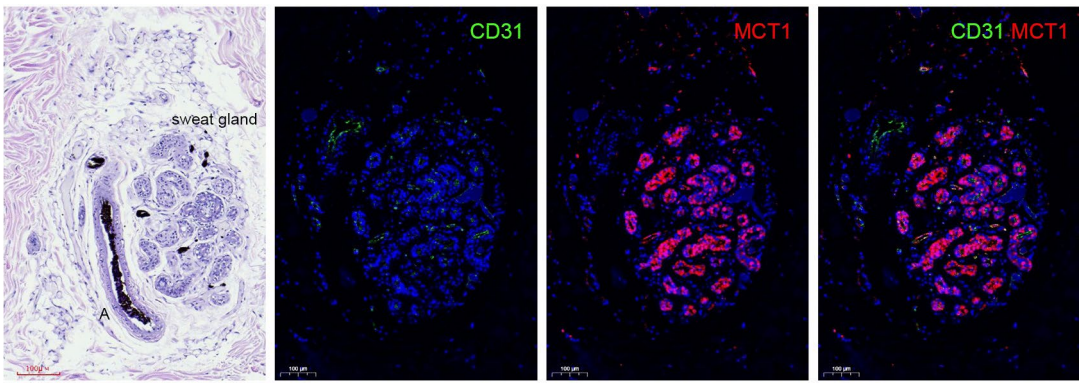

Fig. 5. Expression of cluster of differentiation 31 (CD31) and monocarboxylate transporter 1 (MCT1) in microarterioles and sweat glands. The microarterioles exhibit positive staining for CD31 but are negative for MCT1. In contrast, the sweat gland tissue shows positive staining for MCT1. CD31: cluster of differentiation 31; MCT1: monocarboxylate transporter 1.

In this study, we used lead oxide-gelatin and latex for intravascular dual perfusion to label and analyze the characteristics of microarterioles and microvenules in different dermal layers, offering new insights into skin microcirculation structure and function. These findings suggest several interpretations. First, the significant differences in microarteriole and microvenule diameters between the superficial and deep dermis indicate that vessel size adapts to hemodynamic conditions. The larger diameters of both microarterioles and microvenules in the deep dermis likely help accommodate increased blood volume and reduce resistance. Microvenules, with their larger diameters, are suited for collecting and draining blood under lower pressures, while the smaller microarterioles maintain higher pressure gradients essential for effective perfusion[75,76]. Second, the study highlights significant differences in vessel wall thickness across dermal layers and between vessel types. The thicker walls of both microarterioles and microvenules in the deep dermis suggest an adaptation to the higher mechanical demands of this region. Microarterioles consistently have thicker walls than microvenules, which supports their role in maintaining higher blood pressure and controlling flow. In contrast, the thinner walls of microvenules facilitate venous return at lower pressures[77].Third, microvascular density differs significantly

between the superficial and deep dermis. Both microarterioles and microvenules are denser in the superficial dermis, reflecting the higher demand for nutrient exchange, thermoregulation, and oxygen delivery, given its proximity to the epidermis. The lower vascular density in the deep dermis is likely due to reduced metabolic demands, where structural support is more important than direct metabolic exchange. The greater abundance of microvenules relative to microarterioles aligns with their drainage function, emphasizing their role in managing blood flow and waste removal[78–81]. Finally, the consistent microarteriole-to-microvenule ratio between the superficial and deep dermis suggests a stable vascular architecture. This stability ensures an effective blood supply and drainage across dermal layers, regardless of depth. Such a balanced ratio helps maintain consistent hemodynamic flow and adapt to variations in physiological needs[24,82]. Together, these findings highlight the structural variations within the dermal microcirculatory network. The observed differences in diameter, wall thickness, and density support a coordinated system of blood supply, pressure regulation, and drainage, tailored to meet the diverse needs of dermal regions, offering insights for guiding frontal flap surgeries and managing complications.

Next, adjacent sections to the H&E-stained slides were subjected to immunofluorescence staining for CD31 and MCT1 to assess their capacity to differentiate between microarterioles and microvenules. CD31, also known as platelet endothelial cell adhesion molecule-1, is a well-established marker for microvascular structures and is predominantly expressed on the surface of vascular endothelial cells, where it participates in endothelial junction formation and angiogenesis[83]. MCT1, encoded by the solute carrier family 16 member 1 (SLC16A1) gene, facilitates the transport of short-chain monocarboxylates, such as L-lactate, pyruvate, and ketone bodies, essential for energy balance and pH regulation[84]. In this study, CD31 was detected in both microarterioles and microvenules, whereas MCT1 was exclusively expressed in microvenules. As mentioned earlier, MCT1 plays a crucial role in proton-coupled transport, which is vital for metabolic, pH, and energy regulation[84]. In skin microcirculation, blood in the microarterioles flows through the capillary network, where material exchange occurs, leading to the accumulation of acidic byproducts such as lactate and pyruvate in the microvenules. These metabolites likely require MCT1-mediated transport, explaining the positive staining for MCT1 in microvenules but not in microarterioles. Interestingly, partial MCT1 positivity was also observed in sweat glands. Human sweat contains approximately 0.1% lactic acid, 0.04% citric acid, 0.0096% acetic acid, and 0.0062% propionic acid. When body temperature rises or during emotional stress, the sympathetic nervous system stimulates the sweat glands, facilitating the transport of these metabolites from the blood into the sweat gland lumen, where they form sweat[85,86]. Due to the high density of sweat glands in the forehead, non-specific MCT1 staining outside the microvenules may be observed[87,88]. In contrast, areas with fewer sweat glands, such as the back or limbs, may produce clearer microvenule staining[89].

This study represents the first use of intravascular dual perfusion to examine the characteristics and spatial distribution of microarterioles and microvenules in the human dermis. It is also the first to employ immunofluorescence staining to differentiate between these vessel types. However, several limitations should be noted. The small sample size limits the generalizability of the findings and may not fully capture the microvascular characteristics of a broader population. Additionally, the focus on forehead skin, chosen for its relevance in reconstructive surgery, may be influenced by the high density of sweat glands, making these findings less applicable to other anatomical regions. Furthermore, technical limitations prevented a detailed investigation of capillary characteristics. Future studies should include larger sample sizes and explore a wider range of anatomical regions, particularly those with fewer sweat glands, as autofluorescence from sweat glands could interfere with immunofluorescence results[90]. Optimizing experimental conditions—such as adjusting antibody concentrations, extending incubation times, lowering temperatures, and using blocking agents—could reduce non-specific staining and improve MCT1 binding specificity to microvenules[91,92]. Moreover, the use of specific markers like neuron-glial antigen 2(NG2) for pericytes and alpha-smooth muscle actin (α-SMA) for vascular smooth muscle cells could enhance our understanding of vessel wall thickness and its relationship with perivascular cell types[93]. This approach would help distinguish microarterioles from capillaries and provide insights into pericyte coverage ratios across different vessel types. By integrating intravascular perfusion and immunofluorescence techniques with these markers, we could gain a more detailed understanding of the capillary network in skin microcirculation, advancing our knowledge of its structure and function. Additionally, future research should focus on using specific immunofluorescent antibodies for microarterioles and/or microvenules in intravascular perfusion, combined with whole-mount immunofluorescence staining. This approach promises to provide a more comprehensive and long-range view of skin microcirculation. The integration of tissue-clearing optical techniques will also significantly enhance our ability to visualize microvascular networks in unprecedented detail, paving the way for deeper insights into the complexities of skin microcirculation[94,95].

In conclusion, our study highlights significant differences in the distribution of microvessels between the superficial and deep dermal layers of the human forehead. We identified MCT1 as a specific marker for microvenules and introduced an innovative method combining CD31 and MCT1 immunofluorescence to differentiate dermal microarterioles from microvenules. These findings improve our understanding of skin microcirculation, with future research focusing on advanced imaging techniques and specific markers to provide deeper insights into its structure and function.

Data availability

The datasets generated during the current study are available from the corresponding author on reasonable request.

Received: 30 October 2024; Accepted: 10 March 2025
Published online: 21 March 2025

References

1. Choi, W. et al. Three-dimensional multistructural quantitative photoacoustic and US imaging of human feet in vivo. *Radiology* **303**, 467–473 (2022).
2. Mauricio, D., Gratacòs, M. & Franch-Nadal, J. Diabetic microvascular disease in non-classical beds: The hidden impact beyond the retina, the kidney, and the peripheral nerves. *Cardiovasc. Diabetol.* **22**, 314 (2023).
3. Casanova, F. et al. Weight change and sulfonylurea therapy are related to 3 year change in microvascular function in people with type 2 diabetes. *Diabetologia* **63**, 1268–1278 (2020).
4. Amson, H. et al. Core-to-skin temperature gradient measured by thermography predicts day-8 mortality in septic shock: A prospective observational study. *J. Crit. Care* **60**, 294–299 (2020).
5. Dolgyras, P. et al. Microcirculation dynamics in systemic vasculitis: Evidence of impaired microvascular response regardless of cardiovascular risk factors. *Rheumatology (Oxford)* **62**, 2510–2516 (2023).
6. Fusco, E. et al. Preclinical vascular alterations in obese adolescents detected by laser-doppler flowmetry technique. *Nutr. Metab. Cardiovasc. Dis.* **30**, 306–312 (2020).
7. Soulaidopoulos, S. et al. Arterial stiffness correlates with progressive nailfold capillary microscopic changes in systemic sclerosis: Results from a cross-sectional study. *Arthritis Res. Ther.* **21**, 253 (2019).
8. Loite, U. et al. The expression pattern of genes related to melanogenesis and endogenous opioids in psoriasis. *IJMS* **22**, 13056 (2021).
9. Piette, Y. et al. Standardised interpretation of capillaroscopy in autoimmune idiopathic inflammatory myopathies: A structured review on behalf of the EULAR study group on microcirculation in rheumatic diseases. *Autoimmun. Rev.* **21**, 103087 (2022).
10. Anyfanti, P. et al. Skin microcirculation dynamics are impaired in patients with rheumatoid arthritis and no cardiovascular comorbidities. *Clin. Exp. Rheumatol.* **41**, 1507–1515 (2023).
11. Alexandrou, M.-E. et al. Haemodialysis and peritoneal dialysis patients have severely impaired post-occlusive skin forearm vasodilatory response assessed with laser speckle contrast imaging. *Clin. Kidney J.* **14**, 1419–1427 (2021).
12. Bouman, E. J. et al. Skin microvascular function and renal hemodynamics in overweight patients with type 2 diabetes: A cross-sectional study. *Microcirculation* **28**, e12700 (2021).
13. Siquier-Dameto, G., Boadas-Vaello, P. & Verdú, E. Intradermal treatment with a hyaluronic acid complex supplemented with amino acids and antioxidant vitamins improves cutaneous hydration and viscoelasticity in healthy subjects. *Antioxidants* **13**, 770 (2024).
14. Wang-Evers, M. et al. Assessing the impact of aging and blood pressure on dermal microvasculature by reactive hyperemia optical coherence tomography angiography. *Sci. Rep.* **11**, 13411 (2021).
15. Liu, X., Michael, S., Bharti, K., Ferrer, M. & Song, M. J. A biofabricated vascularized skin model of atopic dermatitis for preclinical studies. *Biofabrication* **12**, 035002 (2020).
16. Wu, H. et al. Trehalose promotes the survival of random-pattern skin flaps by TFEB mediated autophagy enhancement. *Cell Death Dis.* **10**, 483 (2019).
17. Xiong, J. et al. Comparison of proangiogenic effects of adipose-derived stem cells and foreskin fibroblast exosomes on artificial dermis prefabricated flaps. *Stem Cells Int.* **2020**, 1–14 (2020).
18. Rah, D. K., Yun, I. S., Yun, C.-O., Lee, S. B. & Lee, W. J. Gene therapy using hepatocyte growth factor expressing adenovirus improves skin flap survival in a rat model. *J. Korean Med. Sci.* **29**, S228 (2014).
19. Fujiwara, M. et al. Delayed distally based sural flap with temporary venous supercharging. *Microsurgery* **33**, 534–538 (2013).
20. Frommer, S. A., Teal, L. N., Myers, R. P., Kelley, P. K. & Henry, S. L. Extending the reach of craniofacial free flaps using the descending branch of the lateral circumflex femoral vessels. *Plast. Reconstr. Surg.* **147**, 260e–264e (2021).
21. Salibian, A. A., Swerdlow, M. A., Kondra, K. & Patel, K. M. the free superficially based low-abdominal mini flap for oncoplastic breast reconstruction. *Plast. Reconstr. Surg.* **152**, 959–962 (2023).
22. Tracy, L. E., Minasian, R. A. & Caterson, E. J. Extracellular matrix and dermal fibroblast function in the healing wound. *Adv. Wound Care (New Rochelle)* **5**, 119–136 (2016).
23. Driskell, R. R. et al. Distinct fibroblast lineages determine dermal architecture in skin development and repair. *Nature* **504**, 277–281 (2013).
24. Woodley, D. T. Distinct fibroblasts in the papillary and reticular dermis. *Dermatol. Clin.* **35**, 95–100 (2017).
25. Keith, J. et al. Collagenosis of the deep medullary veins: An underrecognized pathologic correlate of white matter hyperintensities and periventricular infarction?. *J. Neuropathol. Exp. Neurol.* **76**, 299–312 (2017).
26. Moody, D. M., Brown, W. R., Challa, V. R. & Anderson, R. L. Periventricular venous collagenosis: Association with leukoaraiosis. *Radiology* **194**, 469–476 (1995).
27. Pantoni, L. Cerebral small vessel disease: From pathogenesis and clinical characteristics to therapeutic challenges. *Lancet Neurol.* **9**, 689–701 (2010).
28. Goss, J. A. et al. Intramuscular fast-flow vascular anomaly contains somatic MAP2K1 and KRAS mutations. *Angiogenesis* **22**, 547–552 (2019).
29. Deegan, A. J. & Wang, R. K. Microvascular imaging of the skin. *Phys. Med. Biol.* **64**, 07TR01 (2019).
30. Han, T., Sun, B., Wang, W., Cui, J. & Shen, W. The role of ICG angiography in decision making about skin-sparing in pediatric acute trauma. *Front. Pediatr.* **10**, 851270 (2022).
31. Chen, C.-Y. et al. Glucocorticoid-induced loss of beneficial gut bacterial extracellular vesicles is associated with the pathogenesis of osteonecrosis. *Sci. Adv.* **8**, 8eabg335 (2022).
32. Liu, Y. et al. Penetration-enhanced optical coherence tomography angiography with optical clearing agent for clinical evaluation of human skin. *Photodiagn. Photodyn. Ther.* **30**, 101734 (2020).
33. Vanlandewijck, M. et al. A molecular atlas of cell types and zonation in the brain vasculature. *Nature* **554**, 475–480 (2018).
34. Cao, Y., Ao, D.-H., Ma, C., Qiu, W.-Y. & Zhu, Y.-C. Immunoreactivity and a new staining method of monocarboxylate transporter 1 located in endothelial cells of cerebral vessels of human brain in distinguishing cerebral venules from arterioles. *Eur. J. Histochem.* **65**, 3306 (2021).
35. Fan, J. A new technique of scarless expanded forehead flap for reconstructive surgery. *Plast. Reconstr. Surg.* **106**, 777–785 (2000).
36. Manna, F., Guarneri, G. F., Re Camilot, M. D. E. & Parodi, P. C. An easy and cheap way of staining the arterial supply of the face: A preclinical study of visualization of facial vascular territories in human cadavers. *J. Craniomaxillofac. Surg.* **38**, 211–213 (2010).
37. Bergeron, L., Tang, M. & Morris, S. F. A review of vascular injection techniques for the study of perforator flaps. *Plast. Reconstr. Surg.* **117**, 2050–2057 (2006).
38. Moon, E.-H. et al. Essential role for TMEM100 in vascular integrity but limited contributions to the pathogenesis of hereditary haemorrhagic telangiectasia. *Cardiovasc. Res.* **105**, 353–360 (2015).
39. Rees, M. J. W. & Taylor, G. I. A simplified lead oxide cadaver injection technique. *Plast. Reconstr. Surg.* **77**, 141 (1986).
40. Jianbin, T. et al. Improved method of ink-gelatin perfusion for visualising rat retinal microvessels. *Acta Histochem. Cytochem.* **41**, 127–133 (2008).
41. Bouvard, C. et al. Different cardiovascular and pulmonary phenotypes for single- and double-knock-out mice deficient in BMP9 and BMP10. *Cardiovasc. Res.* **118**, 1805–1820 (2022).
42. Kim, Y. H., Choe, S.-W., Chae, M.-Y., Hong, S. & Oh, S. P. SMAD4 deficiency leads to development of arteriovenous malformations in neonatal and adult mice. *J. Am. Heart Assoc.* **7**, e009514 (2018).

43. Long, H.-Q. et al. Value of micro-CT for monitoring spinal microvascular changes after chronic spinal cord compression. *IJMS* **15**, 12061–12073 (2014).
44. Taylor, G. I., Shoukath, S., Gascoigne, A., Corlett, R. J. & Ashton, M. W. The Functional anatomy of the ophthalmic angiosome and its implications in blindness as a complication of cosmetic facial filler procedures. *Plast. Reconstr. Surg.* **146**, 745 (2020).
45. Ashton, M. W., Taylor, G. I. & Corlett, R. J. The role of anastomotic vessels in controlling tissue viability and defining tissue necrosis with special reference to complications following injection of hyaluronic acid fillers. *Plast. Reconstr. Surg.* **141**, 818e–830e (2018).
46. Ueda, M. et al. Combined multiphoton imaging and biaxial tissue extension for quantitative analysis of geometric fiber organization in human reticular dermis. *Sci. Rep.* **9**, 10644 (2019).
47. Aydın, Ç., Couto, J., Giugliano, M., Farrow, K. & Bonin, V. Locomotion modulates specific functional cell types in the mouse visual thalamus. *Nat. Commun.* **9**, 4882 (2018).
48. Braverman, I. M. & Keh-Yen, A. Ultrastructure of the human dermal microcirculation. III. The vessels in the mid- and lower dermis and subcutaneous fat. *J. Investig. Dermatol.* **77**, 297–304 (1981).
49. Braverman, I. M. The cutaneous microcirculation. *J. Investig. Dermatol. Symp. Proc.* **5**, 3–9 (2000).
50. Braverman, I. M. Ultrastructure and organization of the cutaneous microvasculature in normal and pathologic states. *J. Invest. Dermatol.* **93**, 2S-9S (1989).
51. Jung, F. et al. Microcirculation in hypertensive patients. *Biorheology* **50**, 241–255 (2013).
52. Debbabi, H., Bonnin, P., Ducluzeau, P. H., Leftheriotis, G. & Levy, B. I. Noninvasive assessment of endothelial function in the skin microcirculation. *Am. J. Hypertens.* **23**, 541–546 (2010).
53. Stupin, A. et al. Is There association between altered adrenergic system activity and microvascular endothelial dysfunction induced by a 7-day high salt intake in young healthy individuals. *Nutrients* **13**, 1731 (2021).
54. Maréchaux, S. et al. Vascular and microvascular endothelial function in heart failure with preserved ejection fraction. *J. Card. Fail.* **22**, 3–11 (2016).
55. Rossitto, G. et al. Reduced lymphatic reserve in heart failure with preserved ejection fraction. *J. Am. Coll. Cardiol.* **76**, 2817–2829 (2020).
56. Cutolo, M. & Smith, V. Detection of microvascular changes in systemic sclerosis and other rheumatic diseases. *Nat. Rev. Rheumatol.* **17**, 665–677 (2021).
57. Huang, M. et al. Single-cell transcriptomes and chromatin accessibility of endothelial cells unravel transcription factors associated with dysregulated angiogenesis in systemic sclerosis. *Ann. Rheum. Dis.* https://doi.org/10.1136/ard-2023-225415 (2024).
58. Zhang, Y. et al. Factor XII and prekallikrein promote microvascular inflammation and psoriasis in mice. *Br. J. Pharmacol.* https://doi.org/10.1111/bph.16428 (2024).
59. Schaper, N. C., Van Netten, J. J., Apelqvist, J., Lipsky, B. A. & Bakker, K. Prevention and management of foot problems in diabetes: A summary guidance for daily practice 2015, based on the IWGDF guidance documents. *Diabetes Res. Clin. Pract.* **124**, 84–92 (2017).
60. Lee, T.-Y. et al. Skin hydration level cutoff value to predict wound healing potential in diabetic foot ulcers. *Diabetes Res. Clin. Pract.* **193**, 110122 (2022).
61. Martens, R. J. H. et al. Capillary rarefaction associates with albuminuria: The Maastricht study. *JASN* **27**, 3748–3757 (2016).
62. Orbegozo, D. et al. Skin microcirculatory reactivity assessed using a thermal challenge is decreased in patients with circulatory shock and associated with outcome. *Ann. Intensiv. Care* **8**, 60 (2018).
63. Sorrell, J. M., Baber, M. A. & Caplan, A. I. Human dermal fibroblast subpopulations; differential interactions with vascular endothelial cells in coculture: Nonsoluble factors in the extracellular matrix influence interactions. *Wound Repair. Regen.* **16**, 300–309 (2008).
64. Philippeos, C. et al. Spatial and single-cell transcriptional profiling identifies functionally distinct human dermal fibroblast subpopulations. *J. Investig. Dermatol.* **138**, 811–825 (2018).
65. Mauroux, A. et al. Papillary and reticular fibroblasts generate distinct microenvironments that differentially impact angiogenesis. *Acta Biomater.* **168**, 210–222 (2023).
66. Phua, Q. H., Han, H. A. & Soh, B.-S. Translational stem cell therapy: Vascularized skin grafts in skin repair and regeneration. *J. Transl. Med.* **19**, 83 (2021).
67. Schlottmann, F., Strauss, S., Hake, K., Vogt, P. M. & Bucan, V. Down-regulation of MHC class I expression in human keratinocytes using viral vectors containing US11 gene of human cytomegalovirus and cultivation on bovine collagen-elastin matrix (Matriderm®): Potential approach for an immune-privileged skin substitute. *Int. J. Mol. Sci.* **20**, 2056 (2019).
68. Martignago, C. C. S. et al. Preemptive treatment with photobiomodulation therapy in skin flap viability. *J. Photochem. Photobiol. B* **201**, 111634 (2019).
69. Wolff, K.-D. et al. In vivo perfusion of free skin flaps using extracorporeal membrane oxygenation. *J. Craniomaxillofac. Surg.* **48**, 90–97 (2020).
70. Shakouri, A. & Wollina, U. Time to change theory; medical leech from a molecular medicine perspective leech salivary proteins playing a potential role in medicine. *Adv. Pharm. Bull.* **11**, 261–266 (2021).
71. Casal, D. et al. Unconventional perfusion flaps in the experimental setting: A systematic review and meta-analysis. *Plast. Reconstr. Surg.* **143**, 1003e–1016e (2019).
72. Wu, H. et al. Distal arterialized venous supercharging improves perfusion and survival in an extended dorsal three-perforasome perforator flap rat model. *Plast. Reconstr. Surg.* **147**, 957e–966e (2021).
73. Choi, W. J., Reif, R., Yousefi, S. & Wang, R. K. Improved microcirculation imaging of human skin in vivo using optical microangiography with a correlation mapping mask. *J. Biomed. Opt* **19**, 036010 (2014).
74. Weinzierl, A., Harder, Y., Schmauss, D., Menger, M. D. & Laschke, M. W. Boosting tissue vascularization: Nanofat as a potential source of functional microvessel segments. *Front. Bioeng. Biotechnol.* **10**, 820835 (2022).
75. Gutterman, D. D. et al. The human microcirculation: Regulation of flow and beyond. *Circ. Res* **118**, 157–172 (2016).
76. Ellis, C. G., Jagger, J. & Sharpe, M. The microcirculation as a functional system. *Crit. Care* **9**(Suppl 4), S3-8 (2005).
77. Lipowsky, H. H. Microvascular rheology and hemodynamics. *Microcirculation* **12**, 5–15 (2005).
78. Deng, M. et al. Protective effect of fat extract on UVB-induced photoaging in vitro and in vivo. *Oxid. Med. Cell Longev.* **2019**, 6146942 (2019).
79. Krewson, E. A. et al. The proton-sensing GPR4 receptor regulates paracellular gap formation and permeability of vascular endothelial cells. *iScience* **23**, 100848 (2020).
80. Daristotle, J. L. et al. Sprayable and biodegradable, intrinsically adhesive wound dressing with antimicrobial properties. *Bioeng. Transl. Med.* **5**, e10149 (2020).
81. Schencke, C. et al. Morphometric evaluation of wound healing in burns treated with Ulmo (*Eucryphia cordifolia*) honey alone and supplemented with ascorbic acid in guinea pig (*Cavia porcellus*). *Burns Trauma* **4**, 25 (2016).
82. Dayan, L., Brill, S., Hochberg, U. & Jacob, G. Is adenosine a modulator of peripheral vasoconstrictor responses?. *Clin. Auton. Res.* **26**, 141–147 (2016).
83. Zheng, H. et al. Jumonji domain-containing 6 (JMJD6) identified as a potential therapeutic target in ovarian cancer. *Signal Transduct. Target. Ther.* **4**, 24 (2019).
84. Philp, N. J., Wang, D., Yoon, H. & Hjelmeland, L. M. polarized expression of monocarboxylate transporters in human retinal pigment epithelium and ARPE-19 cells. *Invest. Ophthalmol. Vis. Sci.* **44**, 1716 (2003).
85. Wilke, K., Martin, A., Terstegen, L. & Biel, S. S. A short history of sweat gland biology. *Int. J. Cosmet. Sci.* **29**, 169–179 (2007).

86. Zancanaro, C., Merigo, F., Crescimanno, C., Orlandini, S. & Osculati, A. Immunohistochemical evidence suggests intrinsic regulatory activity of human eccrine sweat glands. *J. Anat.* **194**, 433–444 (1999).
87. Yeşilova, Y., Turan, E. & Aksoy, M. Hematidrosis on the forehead following trauma: A case report. *Int. J. Dermatol.* **56**, 212–214 (2017).
88. Hexsel, D. et al. Field effect of two commercial preparations of botulinum toxin type A: a prospective, double-blind, randomized clinical trial. *J. Am. Acad. Dermatol.* **67**, 226–232 (2012).
89. Kirby, N. V. et al. Sex differences in adaptation to intermittent post-exercise sauna bathing in trained middle-distance runners. *Sports Med. Open* **7**, 51 (2021).
90. Chen, X., Gasecka, P., Formanek, F., Galey, J.-B. & Rigneault, H. In vivo single human sweat gland activity monitoring using coherent anti-stokes Raman scattering and two-photon excited autofluorescence microscopy. *Br. J. Dermatol.* **174**, 803–812 (2016).
91. Jiang, X. et al. A circulating, disease-specific, mechanism-linked biomarker for ATTR polyneuropathy diagnosis and response to therapy prediction. *Proc. Natl. Acad. Sci. U. S. A.* **118**, e2016072118 (2021).
92. Moutsiopoulou, A. et al. Bioorthogonal protein conjugation: application to the development of a highly sensitive bioluminescent immunoassay for the detection of interferon-γ. *Bioconjug. Chem.* **28**, 1749–1757 (2017).
93. Bourassa, P., Tremblay, C., Schneider, J. A., Bennett, D. A. & Calon, F. Beta-amyloid pathology in human brain microvessel extracts from the parietal cortex: Relation with cerebral amyloid angiopathy and Alzheimer's disease. *Acta Neuropathol.* **137**, 801–823 (2019).
94. Zhu, J. et al. MACS: Rapid aqueous clearing system for 3D mapping of intact organs. *Adv. Sci. (Weinh)* **7**, 1903185 (2020).
95. Shi, R. et al. A useful way to develop effective in vivo skin optical clearing agents. *J. Biophotonics* **10**, 887–895 (2017).

Acknowledgements
This study is supported by Capital's Funds for Health Improvement and Research (2024-2-4044).

Author contributions
S.R. and Z.C. designed the study. S.R., Z.C., and Y.W. conducted the experiments. Y.W. collected and analyzed the data. L.L. supervised the research. S.R. drafted the manuscript with input from all authors. All authors reviewed and approved the final manuscript.

Declarations

Competing interests
The authors declare no competing interests.

Additional information
Correspondence and requests for materials should be addressed to L.L.

Reprints and permissions information is available at www.nature.com/reprints.

Publisher's note Springer Nature remains neutral with regard to jurisdictional claims in published maps and institutional affiliations.